Identification of Endogenous Adenomatous Polyposis Coli Interaction Partners and β-Catenin-Independent Targets by Proteomics

Popow, Olesja; Paulo, Joao A.; Tatham, Michael; Volk, Melanie; Rojas-Fernandez, Alejandro; Loyer, Nicolas

Published in:
Molecular Cancer Research

DOI:
10.1158/1541-7786.MCR-18-1154

Publication date:
2019

Document Version
Peer reviewed version

Identification of endogenous Adenomatous polyposis coli interaction partners and β-catenin-independent targets by proteomics

Olesja Popow[1,2], João A. Paulo[2], Michael H. Tatham[3], Melanie S. Volk[5], Alejandro Rojas-Fernandez[4], Nicolas Loyer[5], Ian P. Newton[5], Jens Januschke[5], Kevin M. Haigis[1,6], Inke Näthke[5*]

[1]Cancer Research Institute and Department of Medicine, Beth Israel Deaconess Medical Center, Boston, MA 02215, United States

[2]Department of Cell Biology, Harvard Medical School, Boston, MA 02115, United States

[3]Centre for Gene Regulation and Expression, School of Life Sciences, University of Dundee, Dundee, DD1 5EH, Scotland UK

[4]Center for Interdisciplinary Studies on the Nervous System (CISNe) and Institute of Medicine, Universidad Austral de Chile, Valdivia, Chile

[5]Cell and Developmental Biology, School of Life Sciences, University of Dundee, Dundee, DD1 5EH, Scotland UK

[6]Harvard Digestive Disease Center, Harvard Medical School, Boston, MA 02215, United States

Running title: The APC interactome and its β-catenin-independent targets.

Keywords: Adenomatous polyposis coli, destruction complex, colorectal cancer, proteomics, Misshapen-like kinase 1.

Financial Support: Olesja Popow - CRUK PhD fellowship, João A. Paulo - NIH/NIDDK grant K01 DK098285, Michael H. Tatham – supported by CRUK program grant to R. Hay, Alejandro Rojas-Fernandez - FONDECYT 11150532 and PAI79150075, Nicolas Loyer and Jens Januschke - Sir Henry Dale fellowship (Wellcome/Royal Society: 100031Z/12/Z), Kevin M. Haigis - NIH/NCI grant U01CA199252, Ian P. Newton and Inke Näthke – CRUK program grant to Inke Näthke.

Corresponding author: Inke Näthke, Cell and Developmental Biology, University of Dundee, Dow Street, Dundee, DD15EH, Scotland UK. Phone: +44-1382-385821; E-Mail: i.s.nathke@dundee.ac.uk

Conflict of interest disclosure: The authors declare no potential conflicts of interest.

Word count: 6522

1 Table, 6 Figures, 6 Supplementary Figures, 2 Supplementary Tables

Abstract

Adenomatous Polyposis Coli (*APC*) is the most frequently mutated gene in colorectal cancer. APC negatively regulates the Wnt signaling pathway by promoting the degradation of β-catenin, but the extent to which APC exerts Wnt/β-catenin-independent tumor suppressive activity is unclear. To identify interaction partners and β-catenin-independent targets of endogenous, full-length APC, we applied label-free and multiplexed TMT mass spectrometry. Affinity enrichment-mass spectrometry identified more than 150 previously unidentified APC interaction partners. Moreover, our global proteomic analysis revealed that roughly half of the protein expression changes that occur in response to APC loss are independent of β-catenin. Combining these two analyses, we identified Misshapen-like kinase 1 (MINK1) as a putative substrate of an APC-containing destruction complex. We validated the interaction between endogenous MINK1 and APC and further confirmed the negative – and β-catenin-independent – regulation of MINK1 by APC. Increased Mink1/Msn levels were also observed in mouse intestinal tissue and *Drosophila* follicular cells expressing mutant Apc/APC when compared to wild-type tissue/cells. Collectively, our results highlight the extent and importance of Wnt-independent APC functions in epithelial biology and disease.

Implications: The tumor suppressive function of APC - the most frequently mutated gene in colorectal cancer – is mainly attributed to its role in β-catenin/Wnt signaling. Our study substantially expands the list of APC interaction partners and reveals that approximately half of the changes in the cellular proteome induced by loss of APC function are mediated by β-catenin-independent mechanisms.

Introduction

Mutations in *Adenomatous Polyposis Coli* (*APC*) are a frequent (> 80%) and early event in the development of sporadic colorectal cancer (1, 2). Germline mutations in *APC* also form the genetic basis of Familial Adenomatous Polyposis (FAP), an inherited form of the disease that is characterized by hundreds of colorectal polyps that progress to cancerous lesions if left untreated (3). This makes a comprehensive understanding of the normal interactions and functions of APC crucial for effectively targeting *APC* mutant cells.

The tumor suppressive function of APC has been mainly attributed to its role in Wnt signaling. In conjunction with Axin, APC acts as a scaffold for the β-catenin destruction complex, thereby limiting the transcription of pro-proliferative β-catenin target genes in the absence of Wnt ligands (4). The vast majority of *APC* mutations result in the translation of a truncated protein and consequent deregulation of Wnt signaling (1, 2). Nevertheless, Wnt-independent roles of APC likely also contribute to its function as a tumor suppressor. This is exemplified by the rare detection of mutations in other Wnt signaling components, including β-catenin, in colorectal cancer (5). Although deletion of Apc in the intestinal epithelium in mice phenocopies homozygous truncation mutations, it leads to more rapid onset of tumors despite lower levels of Wnt activation (6). It thus emerges that loss of wild-type (WT) APC confers additional advantages to cells beyond β-catenin-mediated proliferation, but the extend of APC's Wnt-independent functions is unclear.

A variety of proteins have been described to interact with APC in addition to β-catenin destruction complex components (7). However, proteome-wide studies of APC-binding proteins are limited to interactome and yeast-two-hybrid experiments with overexpressed, tagged and/or fragments of APC (8-11). Using tagged APC in interaction studies is problematic because the C-terminal PDZ-binding domain must remain free to interact with other proteins (12). Similarly, the N-terminal oligomerization domains rely on coiled-coil formation and may be compromised by N-terminal tags (13). To overcome these limitations, we used label-free affinity-enrichment mass spectrometry (AE-MS) to identify a more comprehensive set of interacting partners of endogenous, non-tagged APC. Furthermore, we applied an untargeted global approach using tandem mass tag (TMT)-based and label-free MS to identify proteins that are regulated by APC in their abundance. These two data sets provide a unique resource for the exploration of Wnt/β-catenin-dependent and independent functions of APC. In addition, we could identify potential targets of APC-containing destruction complexes by combining our data on APC-interacting and APC-regulated proteins (Figure 1A). While no direct evidence for the assembly of such complexes by APC exists, other components of the β-catenin destruction complex, such as GSK-3β and $SCF^{\beta\text{-}TrCP}$, are known to have many targets (14, 15). We thus hypothesized that APC may directly regulate the abundance of other proteins in addition to β-catenin.

Materials and Methods

Cell Culture

Colo320, HeLa, and SW480 cells were obtained from the American Type Culture Collection. U2OS cells were obtained from CRUK. The HCT116-Haβ92 cell line was a kind gift of Todd Waldman, HeLa SEC-C and U2OS SEC-C parental cell lines were a kind gift of Ron Hay, the U2OS Flp-In™ T-Rex™ host cell line was a kind gift of Carol MacKintosh. Cells were grown at 37 °C and 5% CO_2 in Dulbecco's modified eagle medium (DMEM) with 10% fetal bovine serum, 50 U/mL penicillin/streptomycin, and 1% v/v non-essential amino acids (all Thermo Fisher Scientific). HeLa SEC-C, U2OS SEC-C, U2OS Flp-In™ T-Rex™ and cell lines generated from these were grown as described above, with the addition of 100 µg/mL Hygromycin B and 15 µg/mL Blasticidin to the cell culture medium. Cells were culture for a maximum of 20 passages after thawing. Cells were tested for mycoplasma contamination every 6 months using MycoAlert™ (Lonza, Cat# LT-07-418).

Generation of cell lines

U2OS SEC-C MINK1 knockout cell lines

Analysis of the N-terminal coding region of *MINK1* (ensembl ENSG00000141503) predicted potential gRNAs with high target affinity, high efficiency and low off-target scores with binding sites in exon 1 and exon 2 using CRISPR Design. We used the best scoring gMINK1 target site in exon 1 (CGGACAGGTCGATGTCGTCC [AGG]) with a score of 95 and 12 predicted off-target sites in other genes. The gRNA sequence was cloned into pBabeD pU6 and sequence-verified. U2OS cells stably expressing Cas9 (U2OS SEC-C) were co-transfected with 3 µg pBabeD pU6 gMINK1 using Lipofectamine 2000 according to the manufacturer's instructions (Thermo Fisher

Scientific, Cat# 11668027). Cells were grown in DMEM supplemented with 10% FBS, 2 mM L-glutamine, and 100 μg/mL Normocin™ (InvivoGen, Cat# ant-nr-1). After 12 h, medium was replaced with fresh medium with 4 μg/mL Puromycin. After 48 h of selection, 2 μg/mL doxycycline was added to induce Cas9 expression. After 72 h, single cells were sorted with an Influx™ cell sorter (BD Biosciences) into 96-well plates containing DMEM with 20% FBS, 2 mM L-glutamine, 100 U/mL penicillin, 100 μg/mL streptomycin, and 100 μg/mL Normocin™. MINK1 protein expression was screened by western blotting. Genomic DNA of MINK1 KO cells was amplified by PCR and sequenced to confirm the introduction of frameshift mutations.

HeLa SEC-C mNeonGreen-MINK1

The same pBabeD pU6 gMINK1 vector used for the generation of MINK1 knock-out cells was used for the fusion of mNeonGreen to the N-terminus of MINK1 in HeLa SEC-C cells as described previously (16). A donor vector was designed to replace the ATG start codon of *MINK1* with the start codon of an mNeonGreen cDNA cassette, flanked by ~500 bp homology arms. The donor vector was synthesized by GeneArt (Life Technologies). Expression of mNeon-MINK1 in selected and expanded single cell clones was validated by western blotting and microscopy.

U2OS Flp-In T-Rex MINK1-GFP/GFP

Stable cell lines with tetracycline/doxycyline-inducible expression of MINK1-GFP/GFP-MINK1 and GFP, respectively, were generated using the Flp-In™ T-Rex™ System according to the manufacturer's instructions (Thermo Fisher Scientific) by transfecting U2OS Flp-In™ T-Rex™ host cells with pcDNA5 FRT/TO C-GFP, pcDNA5 FRT/TO

MINK1-GFP, or pcDNA5 FRT/TO GFP-MINK1 respectively, and pOG44, a constitutive Flp recombinase expression plasmid.

Generation of fly lines and mosaic follicular epithelia

The YFP-fused, endogenously expressed allele *msn*^{CPTI003908} was recombined with the FRT[82B], *apc1*$^{-}$, *apc2*$^{-}$ chromosome by meiotic recombination. *msn*^{CPTI003908}, FRT[82B], *apc1*$^{-}$, *apc2*$^{-}$ and Hs-*flp* ; Ubi-*PH*$^{PLC\delta1}$*::RFP* ; FRT[82B], Ubi-*nls::RFP* flies were crossed and *apc1-, apc2-* mutant clones in follicular epithelial cells in the resulting progeny were induced by a 2 hour, 37 °C heat-shock at a late (starting to pigment) pupal stage.

Transfections

For siRNA transfections cells were transfected one day after seeding with siGENOME APC siRNA #1-#3 (Dharmacon, Cat# D-003869-05/06/07), Hs_CTNNB1_5 FlexiTube siRNA (Qiagen, Cat# SI02662478), or siGENOME Non-Targeting siRNA #1 (Dharmacon, Cat# D-001210-01-05) using INTERFERin® (Polyplus-Transfection, Cat# 409-10) using 72 ng siRNA/T-25 flask. Colo320 cells were transfected twice on two consecutive days. For plasmid transfections cells were transfected one day after seeding with 4 μg myc-tagged β-catenin constructs (17)/10 cm dish using Fugene® 6 Transfection Reagent (Promega, Cat#2691).

Mice

All mice were obtained from The Jackson Laboratory and bred and maintained in accordance with their recommendations under specific pathogen-free conditions in the

Biological Resource Unit at the University of Dundee. Compliant with the ARRIVE guidelines the project was approved by the University Ethical Review Committee and authorized by a project license under the UK Home Office Animals (Scientific Procedures) Act 1986.

Protein and RNA harvest

To harvest proteins, cells or cryo-pulverized mouse small intestinal tissue were lysed in 50 mM Tris-HCl pH 7.5, 100 mM NaCl, 5 mM EDTA, 5 mM EGTA, 40 mM β-glycerophosphate, 0.5% NP-40, 1 mM sodium fluoride, 0.1 mM sodium orthovanadate, and 10 μg/mL of each leupeptin, pepstatin A, and chymostatin. Lysates were cleared by centrifugation and supernatants were collected for further processing. Total RNA was isolated using the NucleoSpin® RNA II Kit (Machery-Nagel, Cat# 740955.10).

Immunoprecipitations

For APC IPs 40 μl protein G-sepharose (Sigma-Aldrich, Cat# P-3296) was washed with protein lysis buffer and incubated for 12 h with 80 μg (for AE-MS)/20-40 μg (for WB) of ALI-12-28/C-APC 41.1 antibody (both CRUK) or control V5 tag antibody (kind gift of R. Hay) at 4 °C on a rotating wheel. Antibodies were crosslinked to sepharose using bis[sulfosuccinimidyl]suberate (Thermo Fisher Scientific, Cat# 21580). Antibody-crosslinked sepharose was incubated with pooled cell lysates harvested from five 15 cm dishes (AE-MS and validation Co-IPs)/10 mg protein lysate (all other APC Co-IPs) for 12 hours at 4 °C on a rotating wheel.

For GFP IPs 15 μl GFP-Trap®_A beads (Chromotek, Cat# gta-100) were washed twice with PBS and twice with protein lysis buffer. Lysates harvested from one 15 cm dish of U2OS Flp-In T-Rex MINK1-GFP/GFP-MINK1/GFP cells grown for two days in media containing 75 ng/mL Tetracycline was incubated with the beadsfor 4 hours at 4 °C on a rotating wheel.

Beads were washed repeatedly with 20 mM Tris-HCl ph 7.5, 150 mM NaCl, 1 mM EDTA, 0.05% Triton X-100, and 5% glycerol (for APC IPs) or protein lysis buffer (for GFP-IPs). Proteins were eluted by boiling with 1.3x NuPAGE™ LDS sample buffer (Thermo Fisher Scientific, Cat# NP0008).

SDS-PAGE and Western Blotting

Protein samples (50 μg (cell lysates)/100 μg (tissue lysates) were separated on pre-cast NuPAGE™ 4-12% gradient Bis-Tris polyacrylamide protein gels (Thermo Fisher Scientific, Cat# NP0322/NP0321), transferred to nitrocellulose membrane, and blotted with primary antibodies: anti-ABI2 (Cat# 302-499A, RRID: AB_1966095), anti-GIT1 (Cat# 302-101A, RRID: AB_1604200), anti-GIT2 (Cat# 302-103, RRID: AB_1604269), anti-RNF20 (Cat# 300-714A, RRID: AB_533428), anti-hPrp3p (Cat# 302-073A, RRID: AB_1604202), anti-MINK1 (Cat# A302-192A, RRID: AB_1659822), anti-PAK1 (Cat# 301-259A, RRID: AB_890620), anti-PDZ-GEF2 (Cat# 301-967A, RRID: AB_1548003), anti-RNF25 (Cat# 303-844A, RRID: AB_2620195; all Bethyl Laboratories); anti-Aurora B (Cat# ab2254, RRID: AB_302923), anti-CASK (Cat# ab99039, RRID: AB_10696957), anti-LATS1 (Cat# ab70562, RRID: AB_2133360; all Abcam); anti-GAPDH (Millipore, Cat# MAB374, RRID: AB_2107445); anti-GFP (Clontech Laboratories, Cat# 632381;

RRID: AB_2313808); anti-LSM7 (Cat# 18941-1-AP, RRID: AB_10596483), anti-TBP (Cat#66166-1-Ig, both Proteintech) anti-β-catenin (BD Transduction Laboratories, Cat# 610154, RRID: AB_397555); sheep polyclonal anti-GFP (MRC PPU Dundee, S268B); mouse monoclonal anti-APC N-terminus (CRUK, ALI-12-28); rabbit polyclonal anti-APC N-terminus (18); anti-β-catenin (19). Anti-mouse/rabbit Alexa Fluor Plus 800/680-conjugated secondary antibodies (Thermo Fisher Scientific, Cat# A32735, RRID: AB_2633284/Cat# A32730, RRID: AB_2633279/Cat# A32734; RRID: AB_2633283/Cat# A32729, RRID: AB_2633278) were detected and quantified with the Li-Cor Odyssey imaging system and Image Studio Software.

Immunofluorescence and live imaging

Cells

For immunofluorescence, cells grown on collagen-coated No. 1.5 cover glass were fixed for 10 min with -20 °C methanol, permeabilized using 1% NP40 in PBS for 10 min, and incubated with IF blocking buffer (5% normal goat serum, 2% w/v BSA, 0.1% Triton X-100 in 1x PBS) for 30 min at RT. Cells were washed with 0.2% w/v BSA in 1x PBS, in between steps. Anti-MINK1 antibody (Thermo Fisher Scientific, Cat #PA5-28901, RRID: AB_2546377) was diluted 1:250 in blocking buffer without serum and incubated overnight at 4 °C. After repeated washing, cells were incubated for one hour with 20 μg/mL Hoechst 33342 (Invitrogen, Cat# H3570) and Alexa Fluor® 594 anti-rabbit antibody (Thermo Fisher Scientific, Cat #PA5-28901; RRID: AB_2546377) diluted 1:500. Cover slips were mounted onto microscopy slides using 90% glycerol with 0.5% N-propyl gallate. For live imaging, cells were grown on 35 mm glass bottom dishes

(ibidi, Cat# 81418-200) in DMEM without phenol red. Images were acquired with an inverted Nikon Eclipse Ti-E fluorescence microscope equipped with a Hamamatsu ORCA-R^2 digital CCD camera and a Prior Scientific Lumen 200PRO light source, using a Plan Apo 60x NA 1.4 objective lens. Images were acquired with the MetaMorph software (version 7.8.12.0) and without camera binning. 395/25; 480/40; and 545/30 excitation and 460/50; 535/50; and 620/60 emission filters were used for Hoechst, mNeonGreen, and Alexa594. Image brightness and contrast was adjusted equally for each image using Fiji software (20).

Drosophila egg chambers

Msn::YFP-expressing, mosaic *apc1*$^-$, *apc2*$^-$ mutant female flies were dissected 24 hours after hatching. Ovaries dissected in glucose- (1 g/L) and insulin- (0.2 g/L) supplemented Schneider's medium (Lonza, Cat# Iz04-351q) in a 35 mm glass bottom dish into individual ovarioles. Imaging was performed on a SP8 confocal microscope (LEICA) equipped with a 63x NA 1.2 water immersion objective within the hour following dissection. The Nls::RFP marker was used to discriminate *apc1*$^-$, *apc2*$^-$ mutant cells, *apc1*$^+$, *apc2*$^+$ control cells and *apc1*$^-$, *apc2*$^-$ /*apc1*$^+$, *apc2*$^+$ heterozygous control cells. Msn::YFP levels were measured at the interface between cells of the same genotype and, for each egg chamber, normalized to the median value measured at the interfaces between heterozygous control cells.

<u>Cell adhesion assay</u>

96-well plates coated with 10 $\mu g/cm^2$ collagen (Sigma-Aldrich, Cat# 8919) were washed with PBS and incubated for one hour with DMEM + 0.5% bovine serum albumin (BSA)

267 at 37 °C. Cells were detached with 10 mM EDTA in PBS for 10 min at 37 °C, washed
268 twice with DMEM, counted using a Cellometer® Auto T4 bright field cell counter
269 (Nexcelom Bioscience), and diluted to a density of 1×10^5 cells/mL in DMEM + 0.1%
270 BSA. 10,000 cells were added per well and incubated for 1 h at 37 °C. Loosely attached
271 cells were removed by vigorous shaking of the plate for 10 s, and washing with DMEM +
272 0.1% BSA. Adherent cells were fixed with 4% paraformaldehyde for 10 min, washed,
273 and stained for 10 min with 5 mg/mL crystal violet in 2% ethanol. Plates were washed
274 once with water and then dried overnight. Crystal violet stain was solubilized with 200 μl
275 2% SDS/well for 30 min and diluted 1:4 with water. Absorption was measured at 550 nm
276 using a Synergy H1 Hybrid multi-mode microplate reader (BioTek).
277
278 MTT cell proliferation assay
279 Cells were seeded one day after transfection in 96 cells plates with 1×10^5 cells/well.
280 Viable cells was measured using the TACS® MTT Proliferation Assay Kit (Trevigen,
281 Cat# 4890-25-01 and Cat# 4890-25-02).
282
283 Real Time-quantitative PCR (RT-qPCR)
284 cDNA was synthesized using the qScript™ cDNA Synthesis Kit (Quanta Biosciences,
285 Cat# 95047). RT-qPCR reactions were performed in triplicate using PerfeCTa SYBR®
286 Green FastMix (Quanta Biosciences, Cat# 95072) and a CFX Connect™ Real-Time
287 PCR Detection System (Bio-Rad). C_T values obtained for target genes were normalized
288 to *ACTB* and relative mRNA expression was calculated using the Pfaffl method (21).
289 Primer sequences: *ACTB* forward/reverse –

CTGGGAGTGGGTGGAGGC/TCAACTGGTCTCAAGTCAGTG, *AXIN2* forward/reverse: TGGCTATGTCTTTGCACCAG/TGTTTCTTACTGCCCACACG, *CTNNB1* forward/reverse: ATGGCTTGGAATGAGACTGC/TTCCATCATGGGGTCCATAC, *MINK1* forward/reverse: TCAACCTGCTCATCACCATC/TCCACTTCTGGGTCATTGTG.

Protein analysis by mass spectrometry

For label-free MS analysis Co-IP and complete lysate samples were separated by SDS-PAGE and proteins were visualized by Coomassie Blue staining. Gel lanes were subdivided into three parts – gel regions containing co-eluted antibody chains in Co-IP samples were pooled. In-gel tryptic digestion was performed as described previously (22). Peptides solubilized in 1% FA were analyzed by LC-MS/MS on a Q Exactive mass spectrometer (Thermo Scientific) coupled to an EASY-nLC 1000 liquid chromatography system via an EASY-Spray ion source (Thermo Scientific) with a 75 μm × 500 mm EASY-Spray column (Thermo Scientific) heated to 40 °C. An elution gradient duration of 240 min was used, fractionating mostly over the 3-40% acetonitrile range. Data were acquired in the data-dependent acquisition mode. Full scan spectra (300-1800 Th) were acquired with resolution of 70,000 at 400 Th (after accumulation to a target value of 1,000,000 with maximum injection time of 20 ms). The ten most intense ions were fragmented by higher-energy collisional dissociation (HCD) and measured with resolution 17,500 at 200 m/z and a target value of 500,000, with a maximum injection time of 60 ms. Intensity threshold was $2.1e^4$. Unassigned, +1 and >8+ charge peptides were excluded, and peptide matching was set to “preferred”. A 40 second dynamic exclusion list was applied.

For TMT-label MS analysis samples were processed as previously described (23). Two μg of each sample were analyzed on an Orbitrap Fusion Lumos mass spectrometer coupled to a Proxeon EASY-nLC 1200 liquid chromatography pump (both Thermo Fisher Scientific) and a 100 μm × 35 cm microcapillary column packed with Accucore C18 resin (2.6 μm, 150 Å; Thermo Fisher). Peptides were fractionated over a 150 min gradient of 3 – 25% acetronitrile in 0.125% formic acid. An MS^3-based TMT method was used, as described previously (24).

Raw MS data analysis

Raw MS data files were processed using MaxQuant (25, version 1.5.8.3) using default settings. MS/MS spectra were searched against the UniProt human proteome sequence database. The MaxLFQ algorithm was implemented, applying a minimum ratio count of 2. For label-free samples the 'match between runs' option with default settings was enabled. TMT-labelled samples were quantified by reporter ion MS^3 – TMT10plex (Lys & N-terminal 126C-130N), with a reporter mass tolerance of 0.003 Da. One percent FDR filtering was applied at protein and peptide levels.

MS data processing

Further MS data analysis was performed using Perseus (26, version 1.5.8.5). 'Reverse' proteins, proteins 'only identified by site', and all non-human contaminants and human contaminants, except cytoskeletal components, were filtered out. Data were $\log_2$ transformed. The filtered APC AE-MS data set contained 5,571 identified proteins, of which 5,521 were measured. From these only proteins measured in all four replicates of

at least one IP with N-APC, C-APC or control antibody were carried forward (4,016 proteins). Missing values were imputed from a normal distribution using standard settings (width: 0.3 × standard deviation of measured values, down shift: 1.8 in units of standard deviation of measured values).

The filtered label-free proteome data set contained 5,982 identified proteins, of which 4,927 were measured in at least three replicates of at least one condition and only these were used for further analysis. Missing values were imputed from a normal distribution.

The filtered TMT proteome data set contained 6,949 identified proteins, of which 6,923 were measured in all analyzed samples. Only these proteins were used for further analysis.

Enrichment analysis of category terms within the group of potential APC interactors identified by AE-MS (171 proteins) relative to all proteins measured in this experiment (4,016 proteins) was calculated by Fisher Exact Test using default settings with a Benjamini-Hochberg FDR <0.02 used for truncation.

Network generation

The APC interaction network was generated in Cytoscape (27, version 3.5.0) using information on APC interactors listed in the IntAct Molecular Interaction Database and/or BioGRID interaction repository. Low-confidence links (IntAct MI score <0.6), individual nodes detached from the network, and indirect APC interactors with less than two connections were deleted. The network layout was generated using the Weak Clustering algorithm and the IntAct MI score for edge weighting within the Cytoscape Allegro Layout App.

Results

Identification of APC-interacting proteins by affinity enrichment-mass spectrometry (AE-MS)

For our initial discovery experiments, we used HeLa cells, which express relatively high amounts of wild-type APC that can be efficiently depleted by siRNA. This allowed us to measure protein binding to, and regulation by, APC in the same cell line. APC-containing protein complexes were co-immunoprecipitated using two APC-specific monoclonal antibodies that recognize N- and C-terminal domains, respectively. An isotype-matched antibody against the viral V5 peptide was used as control. Co-immunoprecipitation (Co-IP) with each antibody was performed in quadruplicate. Samples were analyzed by label-free tandem mass spectrometry (LC-MS/MS). We only considered the 4,016 proteins that were detected in all four replicates of Co-IP's with either antibody for further analysis. Pearson correlation coefficients >0.9 for label-free quantification (LFQ) intensities measured across replicates and a clear separation of N-APC, C-APC and control Co-IPs by principal component analysis (PCA) indicated good experimental reproducibility (Supplementary Figures S1A and B). Significant enrichment of proteins in APC-specific versus control Co-IPs was determined by considering both permutation-based FDR (<0.01) and LFQ intensity fold-change (Supplementary Figure S1C).

In total, 171 proteins were significantly enriched in APC-specific Co-IPs (Figure 1B and Supplementary Table S1). These proteins will be referred to hereafter as the

382 'APC interactome'. Eighty and 71 proteins were exclusively enriched in either C-APC or
383 N-APC Co-IPs, respectively. Antibody binding to APC is likely affected by protein
384 interactions at domains close to or overlapping with the antibody epitopes. This could
385 explain co-immunoprecipitation of distinct interactors with different APC-specific
386 antibodies. Consistently, C-APC and N-APC antibodies immunoprecipitated
387 overlapping, but distinct, pools of APC that may contain different subsets of binding
388 partners (Supplementary Figure S1D). Twenty proteins, including APC itself, were
389 significantly enriched in both APC Co-IPs and only half of these were previously
390 described APC interactors (28,29; Supplementary Table S1).
391 To rule out a HeLa cell-specific enrichment of proteins in APC Co-IPs, we
392 validated our AE-MS results in the human colon carcinoma cell line HCT116-Haβ92,
393 which are homozygous for wild-type APC and hemizygous for wild-type β-catenin (30).
394 Thirteen of the novel APC-interacting proteins were selected to cover the range of
395 biological functions represented in the data set and based on antibody availability.
396 Consistent with results obtained by AE-MS, 12/13 proteins were enriched in APC Co-
397 IPs in both cell lines (Supplementary Figure S2).
398
399 <u>The APC interactome is enriched for epithelial-specific GO cellular component terms</u>
400 To identify underlying functional patterns, we analyzed the enrichment of gene ontology
401 (GO), protein family (Pfam), and Kyoto encyclopedia of genes and genomes (KEGG)
402 terms in the APC interactome. Thirty-one terms were significantly over-represented
403 (Benjamini-Hochberg FDR <0.02); the majority can be broadly categorized into three
404 cellular processes: (actin) cytoskeleton organization, cell-cell contact establishment, and

RNA processing (Figure 1C, Supplementary Table S1). APC-interacting proteins associated with cytoskeletal organization included known and newly identified interactors, including several SCAR complex components. The enrichment of terms linked to RNA processing is consistent with APC's role as an RNA-binding protein (31). Strikingly, many of the enriched terms are associated with cell-cell contacts and constitute components characteristic of epithelial cells, e.g. "lateral plasma membrane", "tight junctions", and "cell-cell adherens junction".

Generation of an integrated APC interaction network

To understand the relationship between interaction partners, we tested how our interactome integrated into a network of previously identified APC-binding proteins. Our interactome data set overlaid well with, and added substantially to, the network of known APC-binding proteins (Figure 2). The integrated network revealed many direct and indirect high-confidence links between newly identified and known APC interactors suggesting potential APC-interacting protein complexes. In addition to the 'β-catenin destruction complex' cluster, several sub-networks emerged from this analysis. Two of these included proteins associated with 'LSM protein family' and 'SCAR complex', respectively, and both categories were enriched in our APC interactome data set (Figure 1C).

To validate our network analysis, we generated a control network using 171 proteins randomly selected from the APC AE-MS data set. Compared to the random selection, our interactome exhibited superior integration into the network of known APC-binding partners (Supplementary Figure S3).

APC affects the abundance of many proteins independently of β-catenin

Because our APC interactome included many binding partners that appeared unrelated to Wnt signaling components, we aimed to determine whether APC is involved in the regulation of proteins other than β-catenin, and independently of β-catenin-mediated cellular effects. To this end, we depleted APC alone or together with β-catenin from HeLa cells using siRNA and measured changes in protein abundance by mass spectrometry (MS). Cells were harvested 72 hours after transfection and efficient knockdown was confirmed by western blotting (WB, Supplementary Figure S4A). Simultaneous knockdown of APC and β-catenin abrogated β-catenin target gene activation, as verified by the inhibition of *AXIN2* mRNA transcription (Supplementary Figure S4D). For each siRNA combination, we analyzed four and two experimental replicates by label-free and TMT MS, respectively. Downstream analysis was applied to 6,923 proteins measured in all eight samples by TMT MS and 4,927 proteins measured in at least three replicates of at least one condition by label-free MS. Reproducibility between replicates was very good, as indicated by Pearson correlation coefficients >0.97 and a clear separation of distinct siRNA treatments by PCA (Supplementary Figure S4B and C).

To identify proteins that changed in abundance in response to APC depletion, but independently of β-catenin, we compared TMT/LFQ intensities across conditions of all measured proteins to an “ideal” intensity profile of a hypothetical β-catenin-independent APC target. A negative APC target was defined as a protein that increased in abundance in response to APC loss, independently of whether APC was depleted alone

or together with β-catenin, but which protein levels did not change in β-catenin siRNA compared to control siRNA-treated cells (the intensity profile of an “ideal” negative APC target is indicated in red in Figure 3A top right). Conversely, a positive APC target was defined as a protein that decreased in abundance in response to APC depletion, independent of β-catenin status. The 200 proteins with profiles most similar to the ideal negative and positive APC target were selected based on Pearson correlation. Significant β-catenin-independent APC targets were determined by applying an additional cut-off of >1.5 fold-change in APC and APC+β-catenin siRNA-treated samples relative to control with a *q*-value <0.05 (TMT)/0.1 (LFQ). By TMT MS we identified 53 and 85 proteins that significantly increased and decreased, respectively, in response to APC depletion in a β-catenin-independent manner; by LFQ MS 11 proteins increased and 11 decreased (Figure 3A/B and E/G). Four negatively and seven positively regulated proteins were common to both data sets. This group of proteins was not enriched in distinct GO terms (data not shown), but spanned a range of cellular functions including apoptosis, ion transport, actin organization, and proliferation.

To compare APC’s β-catenin-dependent and -independent effects on protein expression, we also identified proteins that changed in abundance in response to APC depletion in a β-catenin-dependent manner. The number of these proteins was similar to those regulated independently of β-catenin: 64 and 37 were negatively regulated, 86 and 103 were positively regulated when detected by TMT and LFQ MS respectively (Figure 3C/D and F/H, Supplementary Table S2).

Some β-catenin-independent APC targets are also deregulated in human cancer

To determine if any of the identified β-catenin-independent APC targets are implicated in colorectal cancer, we compared our results with a dataset describing proteomic changes in human colorectal adenoma and adenocarcinoma compared to healthy mucosa (32). Nineteen proteins present in our APC target list were also found to be dysregulated – in the same direction – in human adenomas and/or carcinomas (Table 1). These results highlight that mis-expression of some proteins in colorectal cancer could be a direct consequence of loss of WT APC rather than deregulated Wnt signaling.

MINK1 interacts with full length and truncated APC

From the group of β-catenin-independent APC targets identified by total proteomics analysis, six were also found to interact with APC. Amongst these, MINK1 stood out as a potentially druggable serine/threonine kinase. We validated the interaction between MINK1 and full-length APC by Co-IP and WB in two cell lines (Figure 4A). In agreement with results obtained by MS, MINK1 was only enriched in Co-IPs with the N-APC antibody (Supplementary Figure S5A). To rule out N-APC antibody cross-reactivity, we repeated the experiment with lysate from APC-depleted cells. Confirming its specific enrichment in APC protein complexes, the amount of co-immunoprecipitated MINK1 correlated with the levels of APC present in IP lysates (Supplementary Figure S5B). Conversely, APC was also enriched in Co-IPs of over-expressed GFP-tagged MINK1 compared to GFP alone (Supplementary Figure S5C). We next tested whether MINK1 could also interact with truncated APC expressed in colorectal cancer cells. MINK1 co-

496 immunoprecipitated with APC fragments in both SW480 and Colo320 cells (Figure 4B).
497 The ~90 kDa N-terminal APC fragment expressed in Colo320 cells retains the armadillo
498 and oligomerization domain, but lacks all β-catenin and Axin binding sites and other C-
499 terminal domains. The ~220 kDa APC fragment expressed in SW480 cells includes the
500 four most N-terminal β-catenin binding sites. These data suggest that the interaction
501 between the two proteins is mediated by domains in the N-terminal third of APC.
502
503 MINK1 is negatively regulated by APC independently of β-catenin
504 Consistent with our proteomics data, MINK1 levels measured by WB significantly
505 increased after 72 h of APC depletion in HeLa and U2OS cells and this accumulation
506 was independent of changes in β-catenin (Figure 4C and Supplementary Figure S5D
507 and S6A). Similar to results obtained with the siRNA pool, transfection with either of the
508 individual APC siRNAs efficiently decreased APC levels and produced a concomitant
509 increase in MINK1 protein (Supplementary Figure S5E). We validated the effect of APC
510 loss on MINK1 levels *in vivo* by measuring protein expression in intestinal tissue from
511 *Apc* mutant and wild-type mice. Mink1 protein was increased by 2.3-fold (±0.4 SD) in
512 $Apc^{Min/+}$ versus control animals (Figure 5A and 5B). In addition, we addressed whether
513 this regulatory relationship is conserved across species. We generated mosaic follicular
514 epithelia in *Drosophila melanogaster* egg chambers carrying clones of
515 double *APC1*, *APC2* mutant cells (marked by loss of NLS::RFP expression). Measuring
516 levels of a YFP-fused Misshapen protein – the closest orthologue in *Drosophila* -
517 (Msn::YFP) using live microscopy revealed that Msn::YFP levels were significantly
518 higher in cells that did not express APC1 and APC2 (Figure 5C-F).

519

520 Parallels between the regulation of MINK1 and β-catenin protein abundance

521 We hypothesized that APC regulates the abundance of MINK1 – similarly to β-catenin –
522 post-transcriptionally. Transfection with APC siRNA resulted in a significant up-
523 regulation of *AXIN2* mRNA, and this increase was efficiently inhibited when APC and β-
524 catenin were depleted simultaneously. In contrast, *MINK1* mRNA increased moderately
525 but changes in *MINK1* mRNA did not correlate with changes in MINK1 protein
526 abundance (Figure 6A and 4C).

527 We further tested whether the degradation of MINK1, similarly to β-catenin, was
528 dependent on the action of an E3 ubiquitin ligase. Treatment with the NEDD8-activating
529 enzyme selective inhibitor MLN4924, which inhibits cullin-RING ubiquitin ligase activity
530 (33), reproducibly induced a two-fold increase in MINK1 after 24 h (Figure 6B and
531 Supplementary Figure S6B).

532

533 MINK1 localizes to cell-cell junctions and enhances cell adhesion and proliferation

534 To address how elevated MINK1 could contribute to cellular processes affected by *APC*
535 mutations, we determined its sub-cellular localization. In agreement with a previous
536 study (34), immunofluorescence staining showed an enrichment of signal in the
537 perinuclear region (Supplementary Figure S6C). Nevertheless, a similar signal was
538 present in MINK1 knockout cells, suggesting cross-reactivity of this MINK1 antibody
539 with Golgi components. Indeed, the MINK1 antibody used for immunofluorescence
540 recognized additional proteins by WB (Supplementary Figure S6D, the MINK1 antibody
541 we used for WB was unsuitable for immunofluorescence).

To overcome this problem, we generated cells expressing endogenously mNeonGreen-tagged MINK1, enabling us to study its localization live in un-fixed cells (Supplementary Figure S6D). Although fluorescence intensity was low, mNeonGreen signal was clearly enriched at tips of protrusions (*) and at lateral plasma membranes (arrow heads) in areas of cell-cell contact (Figure 6C). No signal enrichment was detected in 'free' regions of the plasma membrane without adjoining cells. Consistent with a role for MINK1 in adhesion, overexpression of MINK1 resulted in a significant increase in cell attachment to collagen (Figure 6D and Supplementary Figure S6E). Furthermore, proliferation of colorectal cancer cells in which regulation of MINK1 by APC was lost (Supplementary Figure S6F), was significantly reduced when MINK1 was depleted using siRNA (Figure 6E).

Discussion

We aimed to elucidate – on a global scale – the diverse molecular roles of APC, with an emphasis on its functions beyond the β-catenin destruction complex. To this end, we applied an untargeted approach using label-free and TMT-based MS to assemble an APC interactome and, furthermore, to identify the β-catenin-independent APC-regulated proteome. These data sets provide a useful resource for the identification of proteins that participate in and coordinate Wnt-independent functions of APC.

In contrast to previous interaction studies, we used endogenous, full-length, and non-tagged APC in our AE-MS experiment. The identification of additional PDZ domain-containing APC interaction partners highlighted the benefit of this approach.

565 Strikingly, the APC interactome was highly enriched for proteins that are part of cellular
566 components characteristic for epithelial cells, as well as members of the membrane
567 associated “guanylate kinase” (MAGUK) protein family, and PDZ-domain containing
568 proteins (Figure 1C). MAGUK proteins are implicated in the establishment of epithelial
569 cell polarity (35). Furthermore, the function of APC in epithelia is – at least partly –
570 mediated by PDZ domain-containing proteins (36). In addition, STRIPAK complex
571 components formed a highly connected cluster within the APC interaction network
572 (Figure 2). APC and the STRIPAK component Striatin localize interdependently to cell-
573 cell junctions in epithelial cells and depletion of Striatin and APC affects tight junction
574 organization (8). It is conceivable that binding to APC regulates the sub-cellular
575 localization, activity, and/or expression of these epithelial-characteristic proteins, in turn
576 controlling cellular adhesion and establishment of epithelial polarity. Investigating these
577 interactions further will provide useful insights into the mechanisms that regulate APC
578 function in different tissues and further improve our understanding of the phenotypes
579 associated with APC loss. Such studies could reveal why *APC* germ line mutations in
580 FAP patients result in cancerous lesions of the gut epithelium, while other organs often
581 remain unaffected.

582 Measuring proteome-wide effects of APC loss revealed a set of β-catenin-
583 independent APC targets, supporting a role of APC in the regulation of protein
584 abundance beyond the β-catenin destruction complex (Figure 3). Similar to the effect on
585 β-catenin, depletion of APC resulted in the accumulation of some proteins, while the
586 levels of others were negatively affected, suggesting that APC can also inhibit
587 degradation of some of its targets. Strikingly, the number of proteins regulated by APC

588 independent and dependent of β-catenin was very similar. It is important to
589 acknowledge that untargeted MS is biased towards detection of more abundant
590 proteins. Consistently, many established, but low-abundant, β-catenin targets, such as
591 Myc and Axin2, were not detected and are thus absent from our analysis. However, this
592 bias operates in both sets of targets equally. Changes in the abundance of individual
593 APC targets could result from alterations in PTMs and/or protein stability – as is the
594 case for β-catenin. This is supported by previous findings in *Drosophila*, where loss of
595 APC2 causes proteome-wide and β-catenin-independent changes in post-translational
596 modifications that also affect protein stability of some proteins (37). In addition, effects
597 on transcription may also contribute to the differences in protein abundance observed in
598 our study.

599 Since we have used HeLa cells (which we chose for technical reasons, see
600 Results section) in our discovery MS experiments, we were unable to identify potential
601 APC interacting proteins and/or targets which expression is e.g. restricted to intestinal
602 epithelial cells. This limitation will need to be addressed in future studies - ideally using
603 human/mouse intestinal tissue expressing wild-type and mutant APC.

604 At present, it remains unclear how changes in these APC targets contribute to
605 the functional consequences of APC loss observed *in vivo*. As a first step towards
606 addressing this question, we compared our data set with data describing proteome-wide
607 changes in colon adenomas and carcinomas (32). Several of the β-catenin-independent
608 APC targets we identified were also found to be dysregulated in colorectal adenomas
609 and/or tumors (Table 1). Among these, NDRG1, which was downregulated in APC-
610 depleted cells in our study and also in cancerous tissue, might be of particular interest.

NDRG1 has been established as a tumor suppressor in colorectal cancer cells based on its negative effects on metastasis and apoptosis (38).

Collectively, our results suggest that part of the protein expression changes observed in colorectal cancer are independent of increased Wnt target gene expression. Investigating the functional impact of these changes will further help to elucidate how APC loss contributes to cancer development beyond de-regulated β-catenin. Accounting for these effects will be especially important when considering cancer therapy, as they reveal that consequences of mutant APC protein cannot be fully rectified by restoring normal Wnt signaling.

Little is known about the functions of MINK1 or the regulation of its activity and/or its abundance. Existing data implicate MINK1 in cell adhesion, cell migration and planar cell polarity (PCP; 34,39,40) - processes crucial for epithelial biology. Furthermore, MINK1 kinase activity is required for completion of cytokinesis (41). Importantly, these processes are also deregulated in APC mutant tissues (42-44). Moreover, TRAF2 and NCK-interacting protein kinase (TNIK), which shares high sequence homology with MINK1, is emerging as a promising target for colorectal cancer therapy, as it regulates the activity of the TCF-4/β-catenin transcription complex (45).

Collectively, our results indicate that MINK1 is regulated by APC in a manner similar to β-catenin (Figure 4 and 6). Importantly, increased Mink1/Msn levels after loss of wild-type Apc/APC1,2 were also observed *in vivo*, in mouse intestinal tissue and follicular cells in *Drosophila* (Figure 5). Consistent with its localization to cell-cell junctions, over-expression of MINK1-GFP resulted in increased cell adhesion (Figure

6C, D). This is in contrast to a previous study, in which cells overexpressing full-length MINK1 did not grow in clusters but in isolation, suggesting decreased adhesion between cells (34). However, in this case, the effects were not quantified and additional studies of MINK1 overexpression on cell-cell adhesion do not exist. It is conceivable, that enhanced cell adhesion due to elevated MINK1 expression contributes to the reduced cell migration observed in *APC* mutant tissue (43, 46). Moreover, directionality of cell migration could be disturbed when MINK1 expression is deregulated in response to APC loss. Evidence for a role of mammalian MINK1 in PCP is limited (39); however, a role for its *Drosophila* homologue Msn in epithelial PCP has been firmly established (47). In flies, both Apc and Msn act downstream of Dishevelled, which was described as a 'branchpoint' between the canonical Wnt and the non-canonical PCP pathway (48). Our results indicate that regulation of Msn by APC is conserved in flies (Figure 5C-F), suggesting an additional level of crosstalk between these signaling pathways. Furthermore, knockdown of MINK1 in colorectal cancer cells resulted in a significant reduction in proliferation, comparable to the effect seen with β-catenin depletion (Figure 6E). Future experiments will focus on elucidating the molecular mechanisms of MINK1 regulation by APC and the identification of downstream effectors mediating the effects of MINK1 overexpression on cell adhesion.

Acknowledgments

We would like to acknowledge the Nikon Imaging Center at Harvard Medical School and the Dundee Tissue Imaging Facility at the School of Life Sciences, University of Dundee

(supported by Wellcome grant WT101468) for providing help and equipment for microscopy imaging of cells and live *Drosophila* samples, respectively. Stocks from the Bloomington Drosophila Stock Center, which is supported by NIH grant P40OD018537, were used in this study. We would like to thank C. MacKintosh, G. Murugesan, R. Hay, E. Jaffrey, T. Kurz, and M. Keuss (all University of Dundee) for sharing advice and reagents. For their help in the realization of TMT MS experiments we would like to thank S. Gygi and the Taplin Mass Spectrometry Facility at Harvard Medical School.

References

1. Miyoshi, Y., Nagase H., Ando H., Horii A., Ichii S., Nakatsuru S., Aoki T., Miki Y., Mori T., and Nakamura Y. (1992). Somatic mutations of the *APC* gene in colorectal tumors: mutation cluster region in the *APC* gene. Hum. Mol. Genet. *1*, 229–233.
2. Powell, S.M., Zilz, N., Beazer-Barclay, Y., Bryan, T.M., Hamilton, S.R., Thibodeau, S.N., Vogelstein, B., and Kinzler, K.W. (1992). *APC* mutations occur early during colorectal tumorigenesis. Nature *359*, 235–237.
3. Leoz, M.L., Carballal, S., Moreira, L., Ocaña, T., and Balaguer, F. (2015). The genetic basis of familial adenomatous polyposis and its implications for clinical practice and risk management. Appl. Clin. Genet. *8*, 95–107.
4. Stamos, J.L., and Weis, W.I. (2013). The β-catenin destruction complex. Cold Spring Harb. Perspect. Biol. *5*, a007898.
5. Polakis, P. (2000). Wnt signaling and cancer. Genes Dev. *14*,1837–1851.

6. Cheung, A.F., Carter, A.M., Kostova, K.K., Woodruff, J.F, Crowley, D., Bronson, R.T., Haigis, K.M., Jacks, T. (2010). Complete deletion of Apc results in severe polyposis in mice. Oncogene *29*, 1857-1864.
7. Nelson, S., Näthke, I.S. (2013). Interactions and functions of the Adenomatous polyposis coli (APC) protein at a glance. J. Cell Sci. *126*, 873-877.
8. Breitman, M., Zilberberg, A., Caspi, M., and Rosin-Arbesfeld, R. (2008). The armadillo repeat domain of the APC tumor suppressor protein interacts with Striatin family members. Biochim. Biophys. Acta *1783*, 1792–1802.
9. Bandyopadhyay, S., Chiang, C., Srivastava, J., Gersten, M., White, S., Bell, R., Kurschner, C., Martin, C.H., Smoot, M., Sahasrabudhe, S., et al. (2010). A human MAP kinase interactome. Nature Methods *7*, 801-805.
10. Hein, M.Y., Hubner, N.C., Poser, I., Cox, J., Nagaraj, N., Toyoda, Y., Gak, I.A., Weisswange, I., Mansfeld, J., Buchholz, F., et al. (2015). A human interactome in three quantitative dimensions organized by stoichiometries and abundances. Cell *163*, 712–723.
11. Song, J., Hao, Y., Du, Z., Wang, Z., and Ewing, R.M. (2012). Identifying novel protein complexes in cancer cells using epitope-tagging of endogenous human genes and affinity-purification mass spectrometry. J. Proteome Res. *11*, 5630–5641.
12. Harris, B.Z., and Lim, W.A. (2001). Mechanism and role of PDZ domains in signaling complex assembly. J. Cell Sci. *114*, 3219–3231.

13. Joslyn, G., Richardson, D.S., White, R., and Alber, T. (1993). Dimer formation by an N-terminal coiled coil in the APC protein. Proc. Natl. Acad. Sci. USA 90, 11109–11113.
14. Kim, N.G., Xu, C., Gumbiner, B.M. (2009). Identification of targets of the Wnt pathway destruction complex in addition to beta-catenin. Proc. Natl. Acad. Sci. U S A *106*, 5165-5170.
15. Coyaud, E., Mis, M., Laurent, E.M.N., Dunham, W.H., Couzens, A.L., Robitaille, M., Gingras, A.C., Angers, S., Raught, B. (2015). BioID-based identification of Skp Cullin F-box (SCF)β-TrCP1/2 E3 ligase substrates. Mol. Cell. Proteomics *14*, 1781-1795.
16. Rojas-Fernandez, A., Herhaus, L., Macartney, T., Lachaud, C., Hay, R.T., Sapkota, G.P. (2015). Rapid generation of endogenously driven transcriptional reporters in cells through CRISPR/Cas9. Sci. Rep. *5*, 9811.
17. Aberle, H., Bauer, A., Stappert, J., Kispert, A., Kemler, R. (1997). Beta-catenin is a target for the ubiquitin-proteasome pathway. EMBO J. *16*, 3797-3804.
18. Midgley, C.A., White, S., Howitt, R., Save, V., Dunlop, M.G., Hall, P.A., Lane, D.P., Wyllie, A.H., and Bubb, V.J. (1997). APC expression in normal human tissues. J. Pathol. *181*, 426-433.
19. Hinck, L., Näthke, I.S., Papkoff, J., Nelson, W.J. (1994). Dynamics of cadherin/catenin complex formation: novel protein interactions and pathways of complex assembly. J. Cell Biol. *125*, 1327-1340.

20. Schindelin, J., Arganda-Carreras, I., Frise, E., Kaynig, V., Longair, M., Pietzsch, T., Preibisch, S., Rueden, C., Saalfeld, S., Schmid, B., et al. (2012). Fiji: an open-source platform for biological-image analysis. Nat. Methods *9*, 676-682.
21. Pfaffl, M.W. (2001). A new mathematical model for relative quantification in real-time RT-PCR. Nucleic Acids Res. *29*, e45.
22. Shevchenko, A., Tomas, H., Havlis, J., Olsen, J.V., and Mann, M. (2006). In-gel digestion for mass spectrometric characterization of proteins and proteomes. Nat. Protoc. *1*, 2856-2860.
23. Paulo, J.A., O'Connell, J.D., Everley, R.A., O'Brian, J., Gygi, M.A., and Gygi, S.P. (2016). Quantitative mass spectrometry-based multiplexing compares the abundance of 5000 *S. cerevisiae* proteins across 10 carbon sources. J. Proteomics *148*, 85-93.
24. Paulo, J.P., O'Connell, J.D., and Gygi, S.P. (2016). A Triple Knockout (TKO) proteomics standard for diagnosing ion interference in isobaric labeling experiments. J. Am. Soc. Mass. Spectrom. *27*, 1620-1625.
25. Cox, J., and Mann, M. (2008). MaxQuant enables high peptide identification rates, individualized p.p.b.-range mass accuracies and proteome-wide protein quantification. Nat. Biotechnol. *26*, 1367-1372.
26. Tyanova, S., Temu, T., Sinitcyn, P., Carlson, A., Hein, M.Y., Geiger, T., Mann, M., and Cox, J. (2016). The Perseus computational platform for comprehensive analysis of (prote)omics data. Nat. Methods *13*, 731-740.
27. Shannon, P., Markiel, A., Ozier, O., Baliga, N.S., Wang, J.T., Ramage, D., Amin, N., Schwikowski, B., and Ideker, T. (2003). Cytoscape: a software environment

for integrated models of biomolecular interaction networks. Genome Res. *13*, 2498–2504.

28. Orchard, S., Ammari, M., Aranda, B., Breuza, L. Briganti, L., Broackes-Carter, F., Campbell, N.H., Chavali, G., Chen, C., del Toro, N., et al. (2014). The MIntAct project–IntAct as a common curation platform for 11 molecular interaction databases. Nucleic Acids Res. *42*, D358–D363.
29. Stark, C., Breitkreutz, B.-J., Reguly, T., Boucher, L., Breitkreutz, A., and Tyers, M. (2006). BioGRID: a general repository for interaction datasets. Nucleic Acids Res. *34*, D535–D539.
30. Kim, J.-S., Crooks, H., Dracheva, T., Nishanian, T.G., Singh, B., Jen, J., and Waldman, T. (2002). Oncogenic β-catenin is required for bone morphogenetic protein 4 expression in human cancer cells. Cancer Res. *62*, 2744–2748.
31. Preitner, N., Quan, J., Nowakowski, D.W., Hancock, M.L., Shi, J., Tcherkezian, J., Young-Pearse, T.L., and Flanagan, J.G. (2014). APC is an RNA-binding protein, and its interactome provides a link to neural development and microtubule assembly. Cell *158*, 368–382.
32. Wiśniewski, J.R., Duś-Szachniewicz, K., Ostasiewicz, P., Ziółkowski, P., Rakus, D., and Mann, M. (2015). Absolute proteome analysis of colorectal mucosa, adenoma, and cancer reveals drastic changes in fatty acid metabolism and plasma membrane transporters. J. Proteome Res. *14*, 4005–4018.
33. Soucy, T.A., Smith, P.G., Milhollen, M.A., Berger, A.J., Gavin, J.M., Adhikari, S., Brownell, J.E., Burke, K.E., Cardin, D.P., Critchley, S., et al. (2009). An inhibitor

767 of NEDD8-activating enzyme as a new approach to treat cancer. Nature *458*,
768 732–736.
769 34. Hu, Y., Leo, C., Yu, S., Huang, B.C.B., Wang, H., Shen, M., Luo, Y., Daniel-
770 Issakani, S., Payan, D.G., and Xu, X. (2004). Identification and functional
771 characterization of a novel human misshapen/Nck interacting kinase-related
772 kinase, hMINK beta. J. Biol. Chem. *279*, 54387–54397.
773 35. Caruana, G. (2002). Genetic studies define MAGUK proteins as regulators of
774 epithelial cell polarity. Int. J. Dev. Biol. *46*, 511-518.
775 36. Mimori-Kiyosue, Y., Matsui, C., Sasaki, H., and Tsukita, S. (2007). Adenomatous
776 polyposis coli (APC) protein regulates epithelial cell migration and
777 morphogenesis via PDZ domain-based interactions with plasma membranes.
778 Genes to Cells *12*, 219-233.
779 37. Blundon, M.A., Schlesinger, D.R., Parthasarathy, A., Smith, S.L., Kolev, H.M.,
780 Vinson, D.A., Kunttas-Tatli, E., McCartney, B.M., Minden, J.S. (2016). Proteomic
781 analysis reveals APC-dependent post-translational modifications and identifies
782 novel regulator of β-catenin. Development *143*, 2629-2640.
783 38. Mi, L., Zhu, F., Yang, X., Lu, J., Zheng, Y., Zhao, Q., Wen, X., Lu, A., Wang, M.,
784 Zheng, M., et al. (2017). The metastatic suppressor NDRG1 inhibits EMT,
785 migration and invasion through interaction and promotion of caveolin-1
786 ubiquitylation in human colorectal cancer cells. Oncogene *36*, 4323-4335.
787 39. Daulat, A.M., Luu, O., Sing, A., Zhang, L., Wrana, J.L., McNeill, H., Winklbauer,
788 R., and Angers, S. (2012). Mink1 regulates β-catenin-independent Wnt signaling
789 via Prickle phosphorylation. Mol. Cell Biol. *32*, 173–185.

40. Mikrykov, A., and Moss, T. (2012). Agonistic and antagonistic roles for TNIK and MINK in non-canonical and canonical Wnt signalling. PLoS One *7*, e43330.
41. Hyodo, T., Ito, S., Hasegawa, H., Asano, E., Maeda, M., Urano, T., Takahashi, M., Hamaguchi, M., and Senga, T. (2012). Misshapen-like kinase 1 (MINK1) is a novel component of striatin-interacting phosphatase and kinase (STRIPAK) and is required for the completion of cytokinesis. J. Biol. Chem. *287*, 25019–25029.
42. Wong, M.H., Hermiston, M.L., Syder, A.J., and Gordon, J.I. (1996). Forced expression of the tumor suppressor adenomatosis polyposis coli protein induces disordered cell migration in the intestinal epithelium. Proc. Natl. Acad. Sci. USA *93*, 9588–9593.
43. Mahmoud, N.N., Boolbol, S.K., Bilinski, R.T., Martucci, C., Chadburn, A., and Bertagnolli, M.M. (1997). *Apc* gene mutation is associated with a dominant-negative effect upon intestinal cell migration. Cancer Res. *57*, 5045–5050.
44. Caldwell, C.M., Green, R.A., and Kaplan, K.B. (2007). APC mutations lead to cytokinetic failures in vitro and tetraploid genotypes in *Min* mice. J. Cell Biol. *178*, 1109-1120.
45. Yamada, T., and Masuda, M. (2017). Emergence of TNIK inhibitors in cancer therapeutics. Cancer Sci. *108*, 818-823.
46. Sansom, O.J., Reed, K.R., Hayes, A.J., Ireland, H., Brinkmann, H., Newton, I.P., Battle, W., Simon-Assmann, P., Clevers, H., Nathke, I.S., et al. (2004). Loss of Apc *in vivo* immediately perturbs Wnt signaling, differentiation, and migration. Genes Dev. *18*, 1385-1390.

47. Paricio, N., Feiguin, F., Boutros, M., Eaton, S., and Mlodzik, M. (1999). The *Drosophila* STE20-like kinase Misshapen is required downstream of the Frizzled receptor in planar polarity signaling. EMBO J. *18*, 4669-4678.

48. Wallingford, J.B., and Habas, R. (2005). The developmental biology of Dishevelled: an enigmatic protein governing cell fate and cell polarity. Development *132*, 4421-4436.

49. Tusher, V.G., Tibshirani, R., and Chu, G. (2001). Significance analysis of microarrays applied to the ionizing radiation response. Proc. Natl. Acad. Sci. USA *98*, 5116-5121.

Tables

Table 1. Overlap between β-catenin-independent APC targets identified in this study and proteins mis-expressed in colorectal polyps and/or tumors (31).

Protein name (identified by TMT and/or LFQ)	**Log2 fold change**			**q value**				**Log2 fold change (Wiśniewski et al. 2015 – ref 31)**	
	APC siRNA /control	**β-catenin siRNA /control**	**APC+ β-catenin siRNA /control**	**APC siRNA /control**	**β-catenin siRNA /control**	**APC+ β-catenin siRNA /control**		**polyps /normal**	**tumor /normal**
60S ribosomal export protein NMD3 (TMT/LFQ)	2.79/4.54	0.89/2.62	2.02/3.77	<0.001	0.019/0.027	<0.001		0.67	1.46
Peptidyl-prolyl cis-trans isomerase FKBP10 (TMT/LFQ)	1.16/1.13	0.49/0.74	1.00/1.03	0.004/0.04	0.062/0.238	0.003/0.087		0.06	1.95
Melanoma-associated antigen D2 (LFQ)	1.52	1.04	1.29	0.021	0.09	0.047		1.07	2.21
Nucleolar protein 58 (LFQ)	0.93	0.48	1.03	0.059	0.238	0.098		1.5	1.25
6-pyruvoyl tetrahydrobiopterin synthase (TMT)	1.97	0.51	1.29	<0.001	0.057	0.007		1.67	0.66
Glycerophosphocholine phosphodiesterase GPCPD1 (TMT)	1.46	0.41	0.94	0.012	0.083	0.007		1.34	1.19
Hermansky-Pudlak syndrome 5 protein (TMT)	0.74	0.28	0.67	0.002	0.154	0.011		1.14	0.68
Ubiquitin carboxyl-terminal hydrolase 8 (TMT)	1.04	0.44	0.73	0.003	0.069	0.006		0.58	-0.23
Zinc finger protein 622 (TMT)	1.26	-0.19	0.74	0.006	0.283	0.006		0.44	0.80
Ras-related protein Rab-14 (TMT/LFQ)	-1.77/ -1.48	-0.08/ -0.24	-1.39/ -1.01	<0.001/ 0.025	0.568/ 0.384	<0.001/ 0.086		-0.55	-0.27
Aldehyde dehydrogenase family 1 member A3 (LFQ)	-1.98	-0.58	-1.45	0.009	0.192	0.041		-1.14	-0.69
cAMP-dependent protein kinase type I-alpha regulatory subunit (TMT)	-0.71	0.09	-0.61	0.002	0.518	0.011		-0.77	-1.33

Dolichol-phosphate mannosyltransferase subunit 1 (TMT)	-1.09	-0.07	-0.93	0.004	0.617	0.008		-0.97	0.07
EH domain-containing protein 1 (TMT)	-0.60	-0.20	-0.60	0.006	0.229	0.014		-0.95	-0.78
Ferrochelatase, mitochondrial (TMT)	-1.17	-0.04	-0.71	0.005	0.751	0.011		-0.33	-1.54
Leucine zipper protein 1 (TMT)	-1.73	-0.20	-1.24	<0.001	0.267	0.006		0.85	-0.20
Moesin (TMT)	-1.15	-0.09	-0.79	0.003	0.543	0.006		-0.85	-1.06
Non-histone chromosomal protein HMG-14 (TMT)	-1.28	-0.20	-0.85	0.007	0.247	0.006		-0.81	-0.66
Protein NDRG1 (TMT)	-1.55	-0.41	-1.18	0.010	0.098	0.004		-0.17	-0.67

825

Figure Legends

Figure 1. Identification of APC-interacting and -regulated proteins.

A Experimental Outline. Proteins in APC-containing complexes and changes in protein expression in response to siRNA-mediated depletion of APC and/or β-catenin were analyzed by label-free and TMT-based mass spectrometry. The overlap between the two data sets constitutes potential targets of alternative APC-containing complexes. **B** Proteins significantly enriched in C- and/or N-APC Co-IPs. Log2 fold change in mean LFQ intensities between N-APC Co-IP vs. control IP (*x*-axis) plotted against log2 fold change in mean LFQ intensities between C-APC Co-IP vs. control IP (*y*-axis, n=4 experimental replicates). Significance determined by two-sided t-test with permutation-based FDR <0.01 and s_0 = 2 used for truncation (49). **C** GO, Pfam and KEGG terms significantly enriched in the APC interactome data set. Enrichment calculated by Fisher Exact Test, significance determined by Benjamini-Hochberg corrected FDR <0.02. Abbreviations: pos. - positive, reg. - regulation, comp.-med. - complex-mediated, nuc. - nucleation, organiz. - organization.

Figure 2. APC interactome network.

Network integrating known (blue), newly identified (orange), and indirect (grey) APC interaction partners. Nodes are labelled with corresponding gene names and node size correlates with degree of connectivity, i.e. number of edges. Components of distinct protein complexes (1, 3-5) and proteins associated with the cytoskeleton (2) cluster together in sub-networks.

Figure 3. β-catenin-dependent and –independent APC targets identified by TMT-label MS (A-D) and label-free MS (E-H).

A/**E** Profiles of z-scored TMT (A) and LFQ (E) intensities of all measured proteins across samples. Protein identified as negative and positive β-catenin-independent APC targets are shown in orange and blue, respectively. Red lines show profiles for hypothetical 'ideal' targets that increase/decrease in response to APC depletion, but irrespective of a change in β-catenin. **B**/**G** Log2 fold change in mean TMT (B) and LFQ (G) intensities between APC siRNA and control siRNA treated samples (*x*-axis) plotted against the log2 fold change in mean intensities between β-catenin+APC siRNA and control siRNA treated samples (*y*-axis). Proteins selected based on their intensity profiles in **A**/**E** are shown in orange and blue, respectively. **C** and **D** Same as A, but for β-catenin-dependent APC targets.

A Profiles of z-scored LFQ intensities of all measured proteins across samples. Protein identified as negative and positive β-catenin-independent APC targets are shown in orange and blue, respectively. Red lines show profiles for hypothetical 'ideal' targets that increase/decrease in response to APC depletion, but irrespective of change in β-catenin levels. **B** Log2 fold change in mean LFQ intensities between APC siRNA and control siRNA treated samples (*x*-axis) plotted against the log2 fold change in mean LFQ intensities between β-catenin+APC siRNA and control siRNA treated samples (*y*-axis). Proteins selected based on their LFQ intensity profiles in **A** are shown in orange and blue, respectively. **C** and **D** Same as A, but showing β-catenin-dependent APC targets.

Figure 4. MINK1 binds to and is negatively regulated by APC.

A Co-IP of MINK1 with full-length, endogenous APC in HeLa and U2OS cells. **B** Co-IP of MINK1 with C-terminally truncated APC in Colo320 and SW480 colorectal cancer cells; both cell lines lack the second WT allele. **C** Changes in MINK1 proteins levels in response to siRNA-mediated depletion of APC and/or β-catenin measured by WB. Shown are means and SD relative to control samples from four independent transfections. Significance relative to control determined by two-way ANOVA followed by Dunnett's multiple comparison test; *: p value < 0.05, **: p value < 0.01.

Figure 5. Mink1/Msn levels increase in response to Apc loss *in vivo*.

A Expression of Mink1 in small intestinal tissue lysate from WT and $Apc^{Min/+}$ mice measured by WB, each lane represents lysate obtained from individual mice. The Apc^{Min} fragment of approximately 90 kDa was present in mutant mice, but full-length Apc (~310 kDa) was not detectable. **B** Quantification of WB shown in A. Shown is the mean WB signal across the four mice per genotype relative to the signal in WT mice and normalized to Gapdh. Significance relative to WT samples determined by un-paired, two-tailed t test; p value: * < 0.05, ** < 0.01. **C** Live stage 8 *Drosophila* egg expressing NLS::RFP and PH::RFP (magenta) under the control of a ubiquitous promoter, and endogenous Msn::YFP (green). Two large *APC1*, *APC2* double mutant clones within the follicular epithelium are identified by the absence of NLS::RFP and delimited by arrowheads. **D** Magnification of one *APC1*, *APC2* double mutant clone displayed in C. **E** Intensity profiles of RFP and Msn::YFP signal along the follicular

epithelium. **F** Msn signal intensity at the interface between *apc1*$^{-}$*, apc2*$^{-}$ / *apc1*$^{+}$*, apc2*$^{+}$ heterozygous cells (HT-ctrl, n=31), *apc1*$^{+}$*, apc2*$^{+}$ / *apc1*$^{+}$*, apc2*$^{+}$ homozygous control cells (HM-ctrl, n=31) and *apc1*$^{-}$*, apc2*$^{-}$ / *apc1*$^{-}$*, apc2*$^{-}$ homozygous mutant cells (HM-mut, n=38), normalized to the signal at heterozygous interfaces. In total ten clones from then different egg chambers were analyzed. Significance determined by two-tailed Mann-Whitney U test: p value: * = 0.0232, *** < 0.00001.

Figure 6. MINK1 localizes to cell-cell junctions and its overexpression enhances cell adhesion.

A mRNA expression of *MINK1*, *CTNNB1*, and *AXIN2* measured by RT-qPCR 48 and 72 h after siRNA transfection. Indicated are mean expression levels relative to *ACTB* expression with SD from four independent transfections. Significance determined by one-way ANOVA followed by Dunnett's multiple comparison test; p value: * < 0.05, ** < 0.01, *** < 0.001. Note, the same HeLa *AXIN2* mRNA quantification data is also shown in Supplementary Figure S4D. **B** MINK1 protein levels in HeLa cells after treatment with neddylation inhibitor MLN4924 [3 μM] as measured by WB. Shown are relative mean signals normalized to DMSO-treated samples with SD from three independent experiments. Significance determined by one-way ANOVA, **: p value < 0.01. **C** Live imaging of HeLa SEC-C cells expressing endogenously mNeonGreen-tagged MINK1. Scale bars: 10 μm. **D** Adhesion assay with U2OS cells overexpressing MINK1-GFP and GFP, respectively. Adhesion to collagen matrix after one hour was quantified by staining of firmly attached cells with Crystal Violet. Indicated is mean absorbance with SD of independent experiments with two different GFP/MINK1-GFP clones and eight technical

replicates/condition. Significance determined by two-way ANOVA followed by Sidak's multiple comparison test; p value: *** < 0.0003. **E** MTT proliferation assay in Colo320 cells treated with siRNA against β-catenin or MINK1. Shown is the mean absorbance from triplicate measurements. Significance relative to control determined by one-way ANOVA followed by Dunnett's multiple comparison test, p value: * < 0.05, ** < 0.01.

Figures

Figure 1

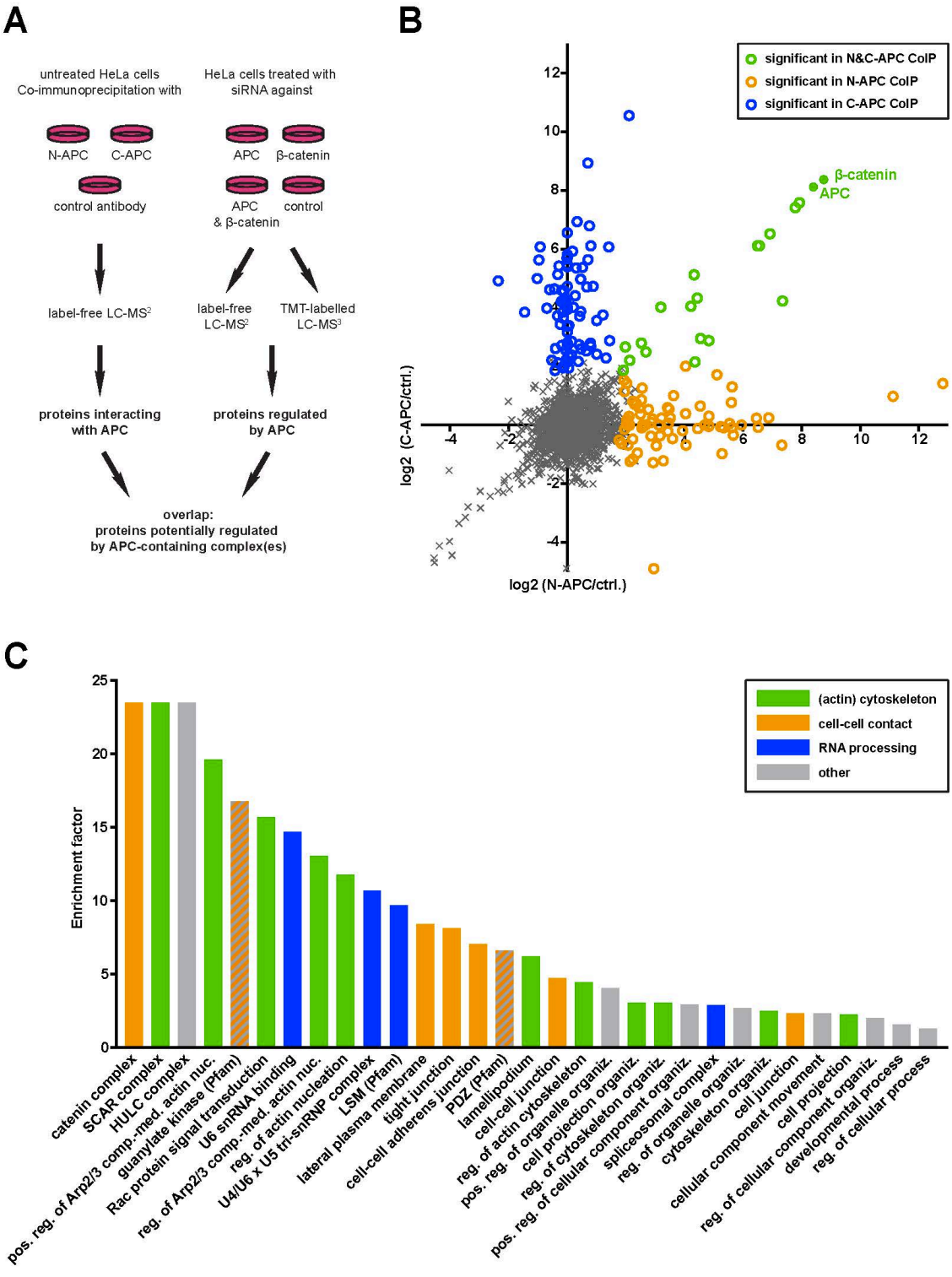

927 Figure 2

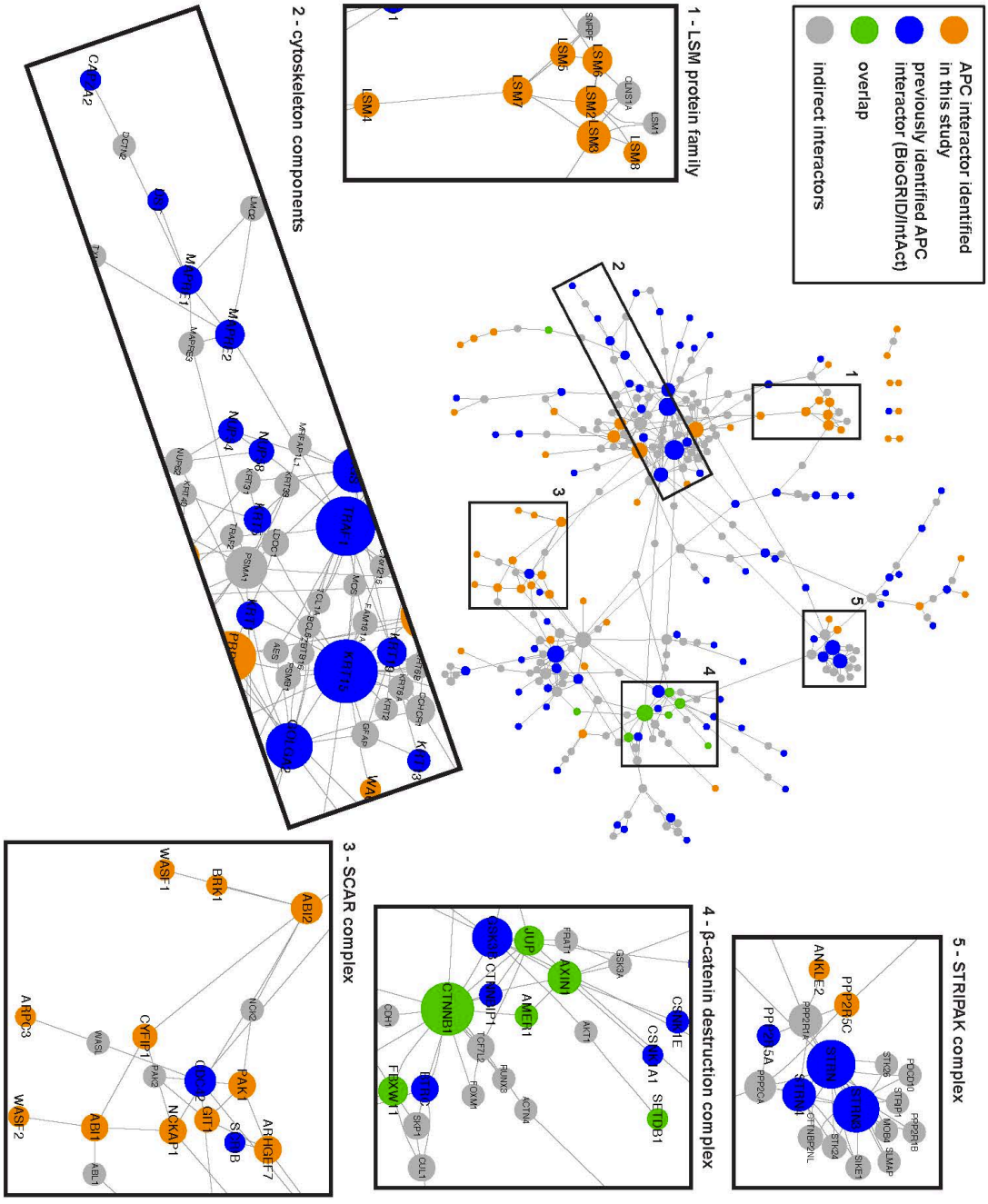

928

929 Figure 3

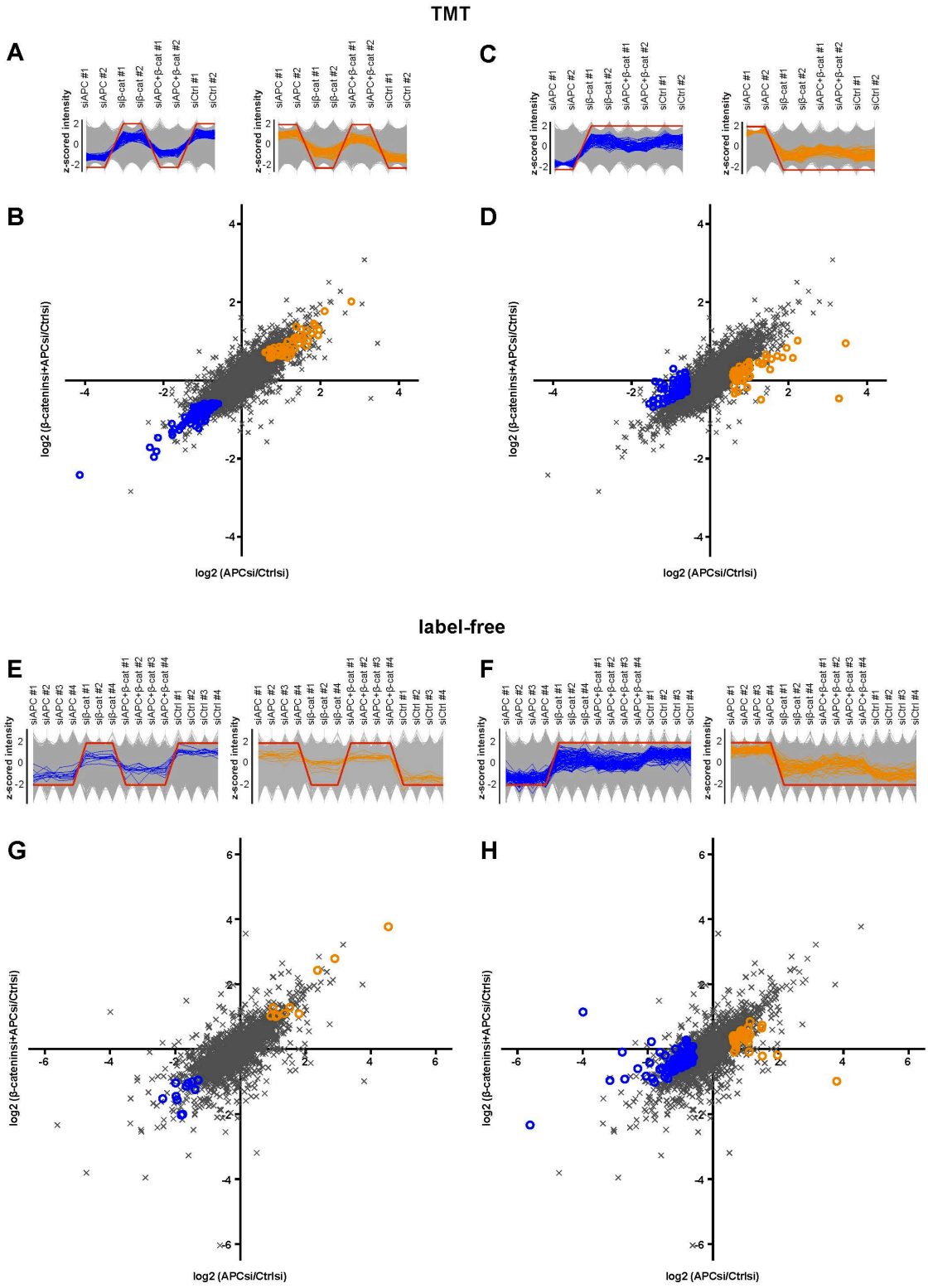

930

931 Figure 4

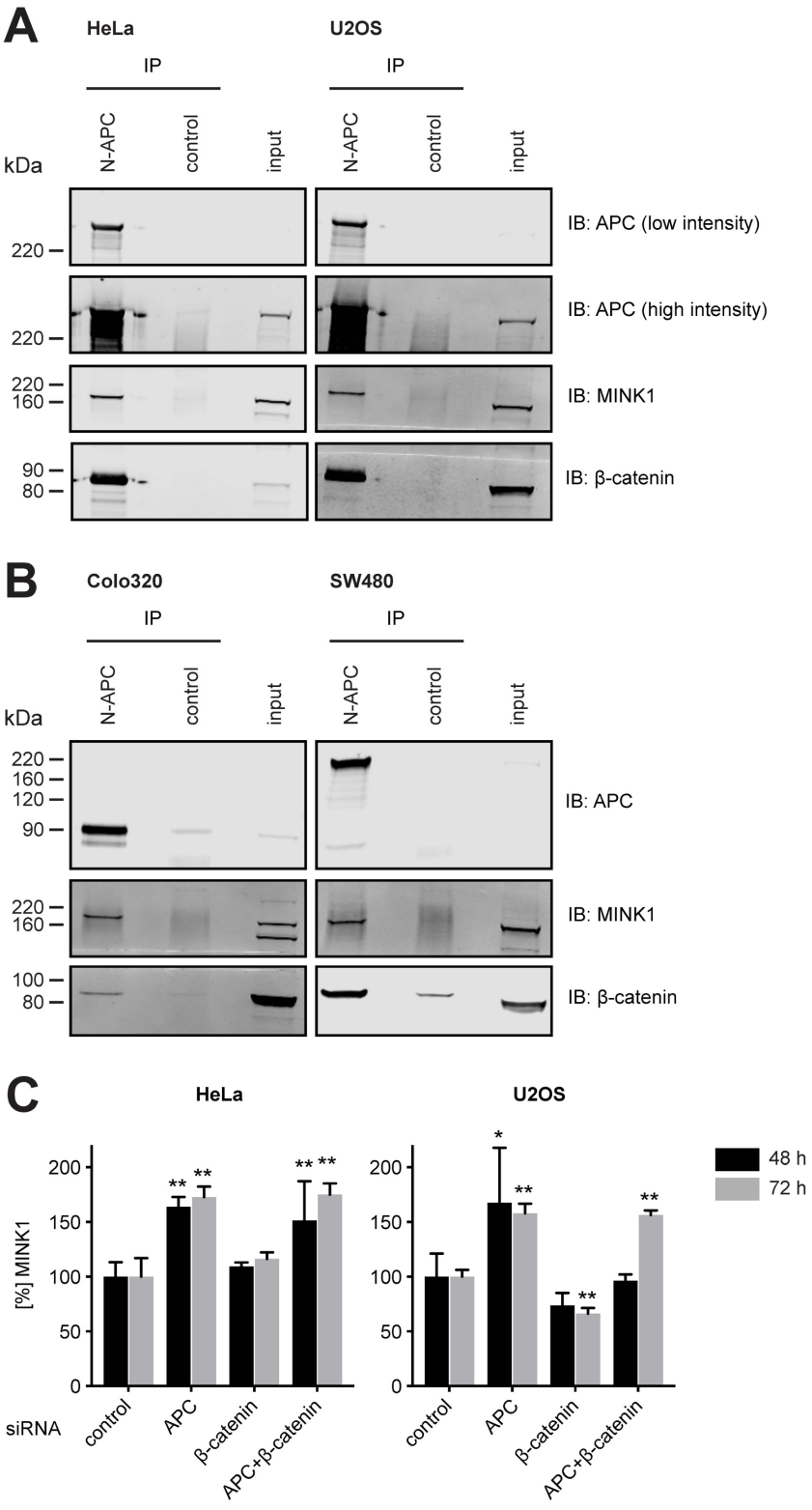
A
HeLa
U2OS
IP
IP
N-APC
control
input
N-APC
control
input
kDa
220
IB: APC (low intensity)
220
IB: APC (high intensity)
220
160
IB: MINK1
90
80
IB: β-catenin
B
Colo320
SW480
IP
IP
N-APC
control
input
N-APC
control
input
kDa
220
160
120
90
IB: APC
220
160
IB: MINK1
100
80
IB: β-catenin
C
HeLa
U2OS
48 h
72 h
[%] MINK1
200
150
100
50
0
siRNA
control
APC
β-catenin
APC+β-catenin

Figure 5

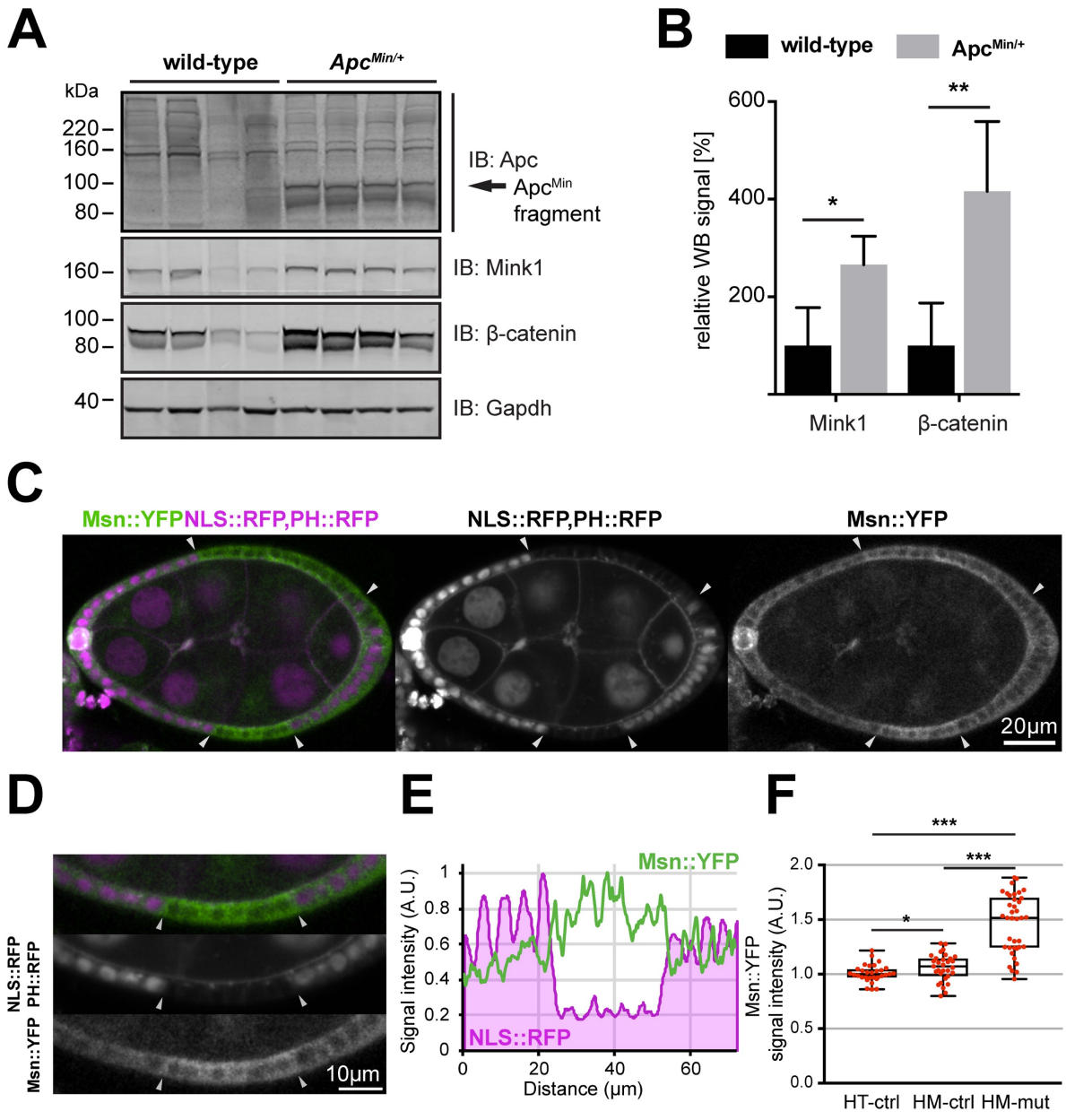
A
wild-type
ApcMin/+
kDa
220
160
100
80
160
100
80
40
IB: Apc
ApcMin
fragment
IB: Mink1
IB: β-catenin
IB: Gapdh
B
wild-type
ApcMin/+
relaltive WB signal [%]
600
400
200
*
**
Mink1
β-catenin
C
Msn::YFP NLS::RFP,PH::RFP
NLS::RFP,PH::RFP
Msn::YFP
20µm
D
NLS::RFP
PH::RFP
Msn::YFP
10µm
E
Msn::YFP
NLS::RFP
Signal intensity (A.U.)
1
0.8
0.6
0.4
0.2
0
0
20
40
60
Distance (µm)
F
***
***
*
Msn::YFP
signal intensity (A.U.)
2.0
1.5
1.0
0.5
0.0
HT-ctrl
HM-ctrl
HM-mut

935 Figure 6

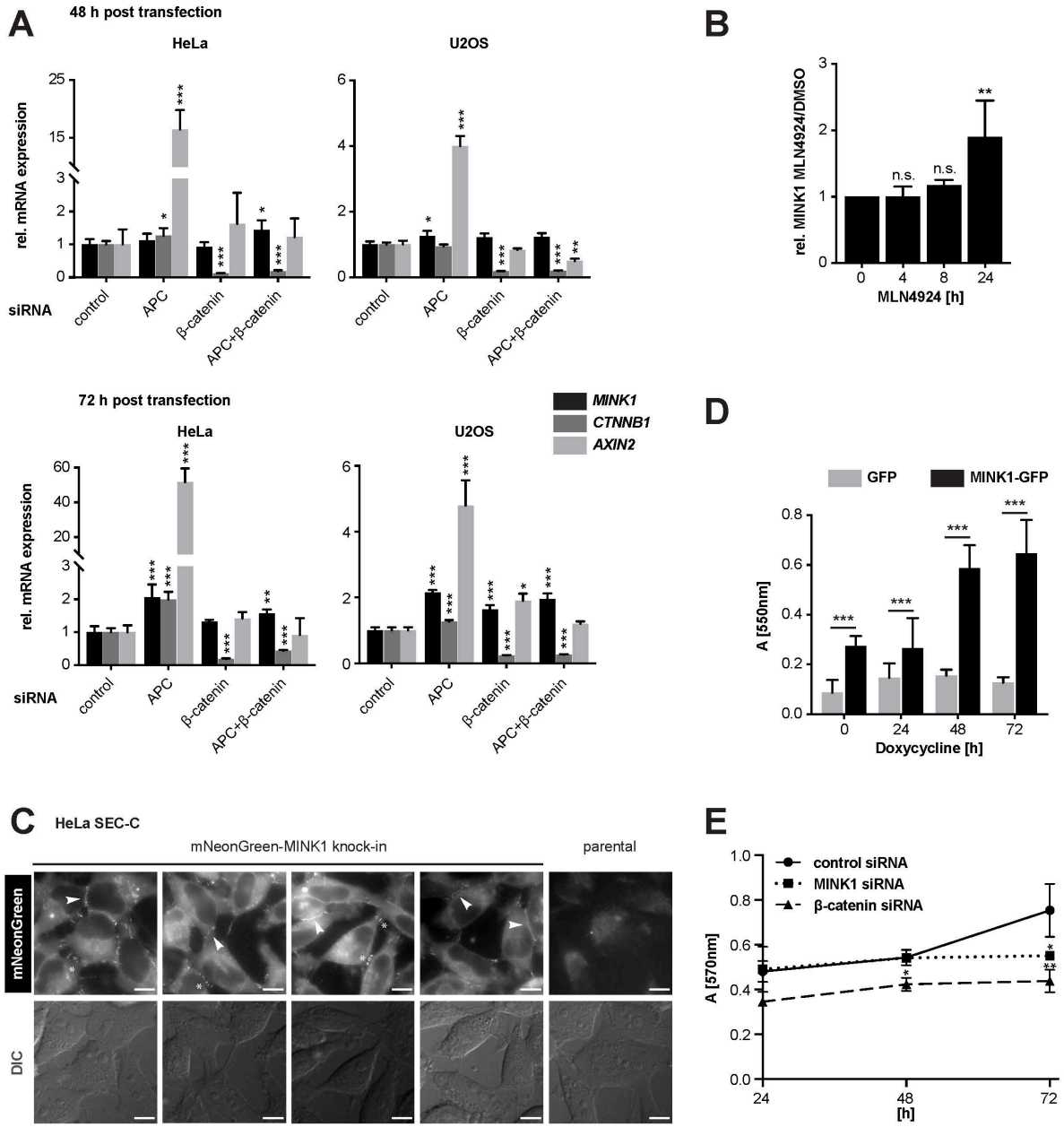

936